Comparative Seismic Analysis of Reinforced Concrete Buildings with Varied Geometry of Structural Members

Elaudlande Joseph[*], Abdulahi Mohamed Gure[**], Ahmad Reshad Noori[***]

[*] Corresponding Author, Specialist, Department of Civil Engineering, Istanbul Gelisim University, Cihangir Mah. Petrol Ofisi Cad. No:3-5, J Block, 34310 Avcilar, Istanbul, Türkiye. E-mail: elaudlande.jos@gmail.com
ORCID: 0009-0007-4011-2057

[**] Specialist, Department of Civil Engineering, Istanbul Gelisim University, Cihangir Mah. Petrol Ofisi Cad. No: 3-5, J Block, 34310 Avcilar, Istanbul, Türkiye. E-mail: abdulahiguure1122@gmail.com
ORCID: 0009-0003-0447-3550

[***] Assoc. Prof. Dr., Department of Civil Engineering, Istanbul Gelisim University, Cihangir Mah. Petrol Ofisi Cad. No: 3-5, J Block, 34310 Avcilar, Istanbul, Türkiye. E-mail: arnoori@gelisim.edu.tr
ORCID: 0000-0001-6232-6303

Received: 05.12.2025 Accepted: 20.02.2026

Abstract

Reinforced concrete (RC) buildings are nowadays commonly used in earthquake regions. However, their seismic performance can vary depending on the geometry and arrangement of structural elements. In this study, the effects of beam, column, slab and shear wall designs on the seismic behavior were examined. The analysis of eight RC building models was done according to the 2018 Turkish Seismic Code by using SAP2000. The dynamic analyses were conducted in order to evaluate: shear forces, inter-story drift, natural vibration periods and required displacements. The results show that even slight geometric modification can have a significant impact on the stiffness, ductility and seismic response of the structure. These analyses helped us to highlight how crucial it is to select the appropriate element geometry in order to increase seismic resilience and design buildings that are more compliant with current standards.

Keywords: Reinforced concrete, SAP2000, Turkish Seismic code, base shear, inter-story drift, structural geometry, seismic analysis.

1. Introduction

Reinforced concrete remains one of the most commonly used materials in construction due to its strength and practical construction options. Since several regions in the world are subjected to seismic hazards, designing earthquake-resistant structures has become one of the most important subjects of study for structural engineers. However, the seismic behavior of reinforced concrete structures depends on the geometry of their structural elements in addition to material properties. Stiffness, ductility, and energy loss are all affected by the size and position of structural elements such as columns, shear walls, beams, and slabs. Even minor modifications to these structural elements can greatly influence the way a building reacts to an earthquake. For this reason, modern seismic codes, like the 2018 Turkish seismic code, have adopted detailed seismic requirements in order to ensure that the buildings satisfy the required strength and deformation capacities. By using advanced modeling tools such as SAP2000, engineers and students can examine different structural modeling under identical loading conditions, at the same time, they are able to obtain a clearer explanation of how geometry affects seismic

performance. Therefore, this approach plays a crucial role in the improvement of RC building design in earthquake regions.

The comparison between several research studies based on global seismic codes shows differences in the way each country establishes its codes and safety requirements. According to Suliman and Lu [1], the most conservative among the African codes they studied was GB-50011. Santo et al. [2] noted that across U.S., European, and other standards, there are variations in structural response because of the differences in response spectrum shape. Rajeev et al. [3], after examination of the Indian code, came to the conclusion that higher base shear and displacement capacity in OMRF structures were found to be required compared to the British and European ones. Kunwar et al. [4] confirmed that the Chinese code contains the most seismic requirements, including base shear values that are higher than those of IS 1893 while Bhavsar et al. [5] noted that Eurocode 8 increased base shear and story drift compared to Indian standards. Eurocode 8 also requires more reinforcement and incorporates bidirectional seismic effects, leading to more conservative designs which was demonstrated by Landingin et al. [6] On the other hand, Ergün et al. [7] demonstrated that buildings designed by following recent Turkish earthquake codes possesses higher seismic capacity. Hasan et al. [8] accentuate the fact that softer soils increase seismic displacements and base shear. Resatoglu and Hamed [9] showed that EC8 and NCSC 2015 have similarity in the base shear results despite the differences in the methodology.

This section sums up some studies comparing structural elements standards. Tabsh [10] concluded that ACI 318 resulted in larger members due to lower strengths. Izhar and Dagar [11] found that Canadian codes required more reinforcement for RC members. Bashir [12] showed that ACI 318M-11 required slightly less reinforcement for short columns compared to BS 8110-97. Kurç et al. [13] proved that there are weaknesses in TEC-07 wall shear design and proposed improvements. Gullu and Mohammed [14] concluded that TS500 provided more reliable shear predictions for RC columns. Amulu and Ezeagu [15] demonstrated that Eurocode 2 produced the highest bending and torsion resistance in RC beams. Uzel [16] improved TS500-2000 shear equations for deep beams. Gowrishankar [17] international seismic codes for safe RC design. Sezen et al. [37] showed that buildings with shear walls performed significantly better during the Kocaeli earthquake. Fragomeni and Loo [38] pointed out that ACMC provisions are suitable for Asian applications. Workeluel et al. [39] demonstrated that ACI 350.3 most accurately captures dynamic effects in elevated RCC tanks.

The analysis of these studies makes us realize that seismic and structural design codes vary from one country to another. Each standard has been established depending on seismic and reinforcement requirements based on the country to obtain a specific performance. We also have to highlight the need to consistently verify the codes, especially regarding shear behavior, material vulnerability and dynamic effects in reinforced concrete systems.
earthquake intensities.

demonstrated that BS 8110 was more economical for UAE construction practices. Nwoji and Ugwu [18] found that Eurocode 2 produced lower span moments and column loads. Zhang et al. [19] found that Chinese codes required less reinforcement than ACI. Algott and Al-Kafri [20] reported that BS 8110 was more economical for short column design. Adhav et al. [21] showed that EN and ACI codes often required more reinforcement than Indian standards. Nwofor et al. [22] concluded that Eurocode 2 is more economical in continuous beam design. Oussadou [23] determined that Eurocode produced economical reinforcement as well for a 50-story building.

Advanced and experimental model observations lead to further conclusions. Jayasinghe et al. [24] found that ANN-based predictions surpassed code formulas for shear behavior. Ahmad et al. [25] confirmed that ANN models accurately predict RC beam behavior. Araújo et al. [26] noted that PCI and Campione-type models performed best for precast corbels. Caterino et al. [27] showed that current code formulas underestimate shear strength in beams without shear reinforcement. Hamrat et al. [28] observed that SFRC beams have higher deflections than predicted by major codes. Lee et al. [29] demonstrated that a simple slab thickness equation exceeded ACI and CSA requirements. Kiani et al. [30] applied FEMA P695 to mixed concrete-steel systems and verified adequate performance. Yang and Ashour [31] found that empirical and strut-and-tie models may become non-conservative for deep beams under certain conditions.

The interpretations of some researchers have been revealed after the study of material innovation. Bernard et al. [32] showed that fiber-reinforced beams can improve crack width predictions when proper inputs are used. Pacheco et al. [33] reported that recycled aggregates increase cracking moment bias in RC beams. Kabashi et al. [34] demonstrated that FRP-reinforced beams behave well under non-strict serviceability conditions. Li et al. [35] discovered that given the fact that prestressed beams are corroded, several codes overestimate their strength.

Studies have been conducted on other structures to add further understandings. Izhar et al. [36] emphasized the importance of understanding

2. Material and Method

This section on elaborates the procedures required by TBDY-2018. It will focus on seismic spectra, analysis steps, and the classification of building.

According to seismic design regulations, building irregularities are categorized into two main types: (A) irregularities in plan layout and (B) irregularities in the vertical direction. These classifications help assess structural performance and the required analysis method under earthquake effects (see Table 1).

The structure is classified as a commercial building with BKS = 3 and an importance factor I = 1.0. Performance objectives are established according to DTS and BYS for the expected earthquake intensities.

Figure 1. Torsional irregularity (A1)

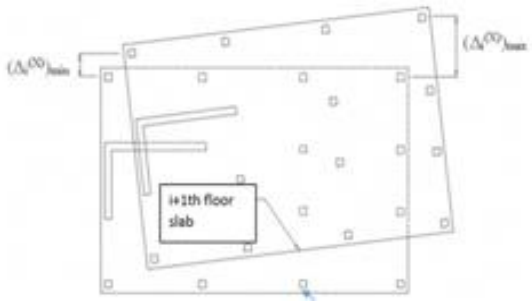

Figure 2. Relative Story Displacements

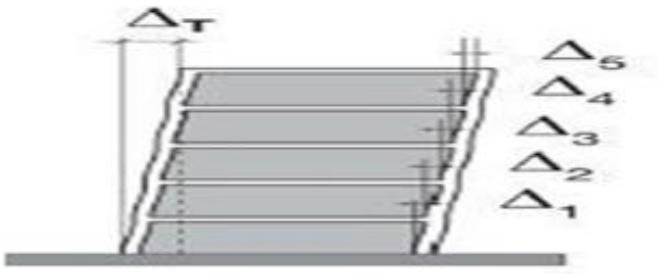

Figure 3. Floor discontinuity (A2)

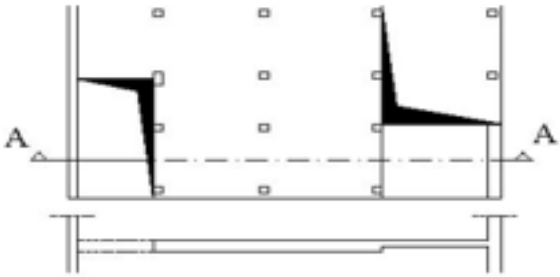

Figure 4. Floor discontinuity (A3)

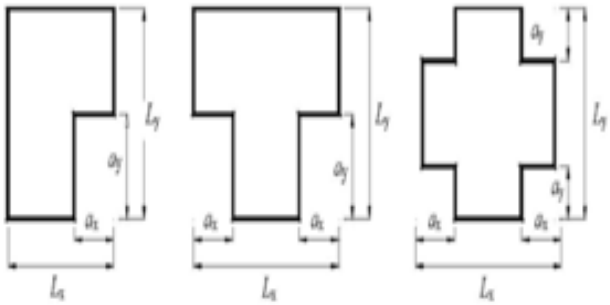

Type	Description	Formula
A1-Torsional Irregularity	Uneven lateral stiffness in plan.	$n_{bi} = \frac{(\Delta_i)_{max}}{(\Delta_i)_{avg}} > 2$ (eq.1)
A2–Floor Discontinuity	Large slab openings or stiffness reductions	$n_{bi} = \frac{\sum_{j=1}^{n} A_{open,i,j}}{A_{floor,i}} > 0.20$ (eq.2)
A3-Plan Projections	Projections or recesses exceed 20% of plan dimensions.	$n_{bi} = \frac{\max(L^{+}_{proj}, L^{-}{}_{proj})}{L_{plan}} > 2$ (eq.3)
B2-Soft story	Drift ratio between adjacent stories exceeds 2	$n_{bi} = \frac{\left(\frac{\Delta_i+1}{h_i+1}\right)_{avg}}{\left(\frac{\Delta_i}{h_i}\right)_{avg}} > 2$ (eq.4)

a) $(\Delta_i)_{max}$: Maximum interstory drift at story i.
b) $(\Delta_i)_{avg}$: Average interstory drift at story i.
c) $A_{open,i,j}$: Area of the j-th slab opening at story i.
d) $A_{floor,i}$: Gross floor slab area at story I before the opening.
e) $L^{+}_{proj}, L^{-}{}_{proj}$: Projection or recess lengths measured from the main plan outline in opposite directions
f) L_{plan}: Total dimension in the same direction in the plan.

For any column or shear wall in the (X) earthquake direction, the reduced interstory drift, denoted as $\Delta_i(x)$, representing the displacement difference between two consecutive stories, is obtained using the following equation. In systems subjected to lateral loads, second-order effects become significant when the normal forces in the columns are also (see Table 2).

Table 2. List of Basic Equations

Feature	Description	Formula
Reduced Inter story Drift	Drift between two consecutive floors in the (X) direction	$\Delta_i^{(x)} = u_i^{(x)} - u_{i-1}^{(x)}$ (Eq.5)
Effective Inter story Drift	Drift normalized by story height	$\delta_i^{(x)} = \Delta_i^{(x)} / h_i$ (Eq.6)
Reduced Drift Using R–I Factors	Relation to behavior and importance factors	$\delta_i^{(x)} = R / I$ (Eq.7)
Drift Limit – Case (a)	Brittle infill walls directly adjacent to frame	$\lambda \frac{\delta_{I,max}^{X}}{h_i} \leq 0.008k$ (Eq.8)
Drift Limit – Case (b)	Flexible joints / independent façade panels	$\lambda \frac{\delta_{I,max}^{X}}{h_i} \leq 0.016k$ (Eq.9)
Material Coefficient k	RC and steel buildings	k = 1.0 (RC), k = 0.5 (Steel)
λ Coefficient	Ratio of DD-3 to DD-2 spectral accelerations at fundamental period	
Second-Order Indicator	P–Δ effect measure at story i	$\theta_{\mathbb{I},i}^{(x)} = \frac{(\Delta_i^{(x)})_{avg} \sum_{k=i}^{N} w_k}{V_i^{(x)} h_i}$ (Eq.10)
Second-Order Limit	Maximum acceptable second-order effect	$\theta_{\mathbb{I},max}^{(x)} \leq 0.12 \frac{D}{C_h R}$ (Eq.3)
Coefficient C_h	Hysteretic behavior coefficient	C_h = 0.5 (RC), Ch = 1 (Steel/composite)
Amplification Factor	Used when second-order limits are exceeded	$\beta_{II}^{(X)} = 0.88 + \frac{C_h}{D} \theta_{II,max}^{(X)} \geq 1$ (Eq.11)
Separation Joint Requirement	Floors aligned	α = 0.25 (R/I)
Separation Joint Requirement	Floors not aligned	α = 0.5 (R/I)

The based shear force **in X direction** can be calculated with:

$$V_{tE}^{(X)} = m_t S_{aR}\left(T_p^X\right) \geq 0.04 m_t I S_{DSg} \quad \text{(Eq.12)}$$

$$m_t = \sum_{i=1}^{N} m_i \quad \text{(Eq.13)}$$

$$S_{aR}(T) = \frac{S_{ae}(T)}{R_a(T)} \quad \text{(Eq.14)}$$

The load reduction factor in (Eq.15)

$$R_a(T) = \begin{cases} R/I & T > T_B \\ D + \left(\frac{R}{I} - D\right) T/T_B \ , & T < T_B \end{cases}$$

Total load distribution:

$$V_{tE}^{(X)} = \Delta F_{NE}^{(x)} + \sum_{i=1}^{N} F_{iE}^{(x)} \quad \text{(Eq.16)}$$

Top floor additional load:

$$\Delta F_{NE}^{(x)} = 0.0075\, N V_{tE}^{(X)} \quad \text{(Eq.17)}$$

Floor-level

$$F_{iE}^{(x)} = \frac{(V_{tE}^{(X)} - \Delta F_{NE}^{(x)}) m_i H_i}{\sum_{j=1}^{N} m_j H_j} \quad \text{(Eq.18)}$$

Rigid diaphragms: Apply $F_{iE}^{(x)}$ at main node.
Non-rigid/irregular floors: Use 2D finite elements.
Plate (membrane) elements:

$$f_{jE}^{(X)} = \frac{f_{iE}^{(X)}}{m_i} m_j^{(s)} \quad \text{(Eq.19)}$$

$$m_j^{(s)} = \frac{m_j^{(s)}}{g}, w_j^{(s)} = w_{G,j}^{(s)} + n w_{Q,j}^{S} \quad \text{(Eq.20)}$$

The tTotal Overturning Moment is

$$M_0^{(X)} = \sum_{i=1}^{N} F_{iE}^{(X)} H_i \quad \text{(Eq.21)}$$

The dominant Natural Vibration Period is

$$T_P^{(X)} = 2\pi \sqrt{\frac{\sum_{i=1}^{N} m_i (d_{fi}^{(X)})^2}{\sum_{i=1}^{N} F_{fi}^{(X)} (d_{fi}^{(X)})}} \quad \text{(Eq.22)}$$

$$T_{PA} = C_t H_N^{3/4} \quad \text{(Eq.23)}$$

RC frames: C_t = 0.1
Steel frames/braced steel: C_t = 0.08
Other structures: C_t = 0.07
RC shear wall buildings:

$$C_t = \frac{0.1}{\sqrt{A_t}} \leq 0.07 \quad \text{(Eq.24)}$$

$$A_t = \sum_j A_{wj} \left[0.2 + \left(\frac{l_{wj}}{H_N}\right)^2\right] \leq \sum_j A_{wj} \quad \text{(Eq.25)}$$

The analyzed workplace buildings are located in Amasya Province, Turkey (Latitude. 40.6502°, Longitude. 35.8286°).

A total of eight distinct buildings were evaluated (8 models). Each building is a six-story reinforced concrete (RC) frame structure composed of beams, columns, shear walls, and slabs. While all buildings share the same general structural system, they differ in their specific dimensions for columns, beams, shear walls, and slabs.

Table 3. The Details for Each Model are Listed

Model	Columns (cm)	Beams (cm)	Shear Wall Thickness (cm)	Slab Thickness (cm)
1	60 × 60	50× 30	30	15
2	70 × 70	50×30	30	15
3	75 × 75	50× 30	30	15
4	60 × 60	60 ×30	30	15
5	60× 60	50 ×35	30	15
6	60 × 60	50 ×30	30	12
7	60× 60	50× 30	35	15
8	60 × 60	50× 25	25	15

3. Numerical Methods and Applications

The materials used are: Concrete Class:C30, reinforcing Steel Grade: S420 and the local soil class has been determined as: ZB. The dead load is G_I = 5.85 KN/m² and the live load is 3 kN/m².

By using SAP2000, the steps will be followed to regenerate the models:

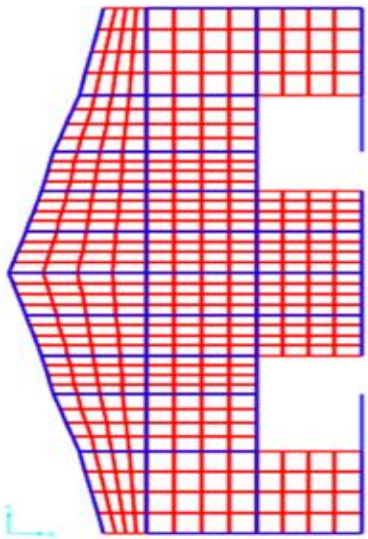

Figure 5. Slab Meshing III from SAP2000

3.1.2. Calculation of Floor Weights

According to TBDY-2018, the live load mass participation coefficient is taken as n = 0.30

Table 4. Floor Weight

Floor no	Wi (kN)
6	6137.82
5	6253.92
4	6253.92
3	6253.92
2	6253.92
1	6253.92

3.1.3. Calculation of the Period Using Modal Analysis

The modal analysis results in the table showed that the fundamental vibration periods remain relatively close across all models, with slight variations reflecting differences in structural stiffness and mass distribution. The first mode gives the highest period values, indicating dominant global flexibility in each model, while higher modes show progressively shorter periods consistent with localized or higher-frequency vibrations. The results demonstrate stable dynamic behavior across the models.

The period of all Models is calculated using SAP2000 (see Table 5).

Table 5. Calculated Periods for Each Model

Period								
Mod	**Model**							
	1	**2**	**3**	**4**	**5**	**6**	**7**	**8**
1	0.623	0.596	0.584	0.557	0.601	0.632	0.602	0.675
2	0.485	0.477	0.473	0.455	0.476	0.490	0.459	0.527
3	0.428	0.419	0.414	0.401	0.420	0.433	0.405	0.468
4	0.173	0.169	0.167	0.161	0.170	0.181	0.172	0.186
5	0.172	0.165	0.165	0.144	0.162	0.177	0.167	0.186
6	0.168	0.165	0.164	0.139	0.157	0.176	0.166	0.182
7	0.167	0.164	0.163	0.138	0.157	0.175	0.165	0.181
8	0.166	0.163	0.163	0.137	0.155	0.174	0.163	0.180
9	0.165	0.163	0.162	0.135	0.154	0.174	0.164	0.179
10	0.164	0.162	0.157	0.135	0.154	0.173	0.163	0.178

The maximum $T_p(X)$ and $T_p(Y)$ value to be considered in the seismic analysis must not exceed 1.4 times the fundamental natural vibration period, TpA, calculated using the empirical formula expressed in equations 22 and 23.

$T_{PA}=C_t H_N^{3/4}$

$T_{pA} = C_t H_N^{3/4} = 0.07 \times 18^{3/4} = 0.611$ sec.

$T_p^{(x)} = 0.4846$ sec ≤ 1.4 $T_{pA} = 0.855$ sec.

$T_p^{(Y)} = 0.601607 \leq 1.4$ $T_{pA} = 0.855$ sec.

Periods calculated for all eight Models and evaluations for their compliance with the conditions specified above are presented in Table 6.

Table 6. Periods with Specific Conditions

Model	$T_p^{(x)}$**(s)**	$T_p^{(Y)}(s)$	$T_{pA}(s)$	**Comment**
1	0.484	0.622	0.855	satisfied
2	0.596	0.477	0.855	satisfied
3	0.473	0.583	0.855	satisfied
4	0.455	0.556	0.855	satisfied
5	0.476	0.601	0.855	satisfied
6	0.490	0.632	0.855	satisfied
7	0.459	0.601	0.855	satisfied
8	0.527	0.675	0.855	satisfied

The preconditions are satisfied and the corner periods of the horizontal design spectrum have been determined.

The horizontal elastic design spectrum was computed using the report obtained from AFAD report (Afet ve Acil Durum Yönetimi Başkanlığı).

For DD2:

$T_A=0.2\frac{S_{D1}}{S_{DS}}$

$T_A=0.2\frac{S_{D1}}{S_{DS}}=0.2\frac{0.255}{0.940}=0.054$ sec.

$T_B=\frac{S_{D1}}{S_{DS}}$

$T_B=\frac{S_{D1}}{S_{DS}}=\frac{0.255}{0.940}=0.271$ sec.

$S_{ae}(T)=\frac{S_{D1}}{T_p^{(Y)}}$ $T_B \leq T \leq T_L$

The vertical elastic design spectral acceleration of Y-direction Model 1 is given as follows:

$S_{ae}(T_p^{(Y)})=\frac{S_{D1}}{T_p^{(Y)}}$ $T_B \leq T_p^{(Y)} \leq T_L$ $S_{ae}(0.6228)=\frac{0.255}{0.6228}$ = 0.4094

The vertical elastic design spectral acceleration of X-direction Model 1 is given as follows.

$S_{ae}(T_p^{(X)})=\frac{S_{D1}}{T_p^{(Y)}}$ $T_B \leq T_p^{(X)} \leq T_L$ $S_{ae}(0.4846)=\frac{0.255}{0.4846}$ = 0.5262

All calculations for eight models are carried out in Excel following the same procedure, and the resulting values are presented in Table 7.

Table 7. DD2 Seismic Parameters Per Model

DD2				
Model	$S_{ae}(T_p^{(X)})$ **(g)**	$S_{ae}(T_p^{(Y)})$ **(g)**	S_{DS}	S_{D1}
1	0.5262	0.4095	0.94	0.255
2	0.42778	0.5349	0.94	0.255
3	0.53922	0.4367	0.94	0.255
4	0.5604	0.4584	0.94	0.255
5	0.53594	0.4242	0.94	0.255
6	0.52032	0.4031	0.94	0.255
7	0.55563	0.4239	0.94	0.255
8	0.48371	0.3775	0.94	0.255

For DD3:

T_A=0.2$\frac{S_{D1}}{S_{DS}}$ =0.2$\frac{0.095}{0.369}$ = 0.052 sec

T_B=$\frac{S_{D1}}{S_{DS}}$=$\frac{0.095}{0.369}$=0.258sec.

The vertical elastic design spectral acceleration of Y-direction Model 1 is given as follows.

$S_{ae}(T_p^{(Y)}) = \frac{S_{D1}}{T_p^{(Y)}}$ $T_B \leq T_p^{(Y)} \leq T_L$

$S_{ae}(0.6228) = \frac{0.095}{0.6228}$ = 0.1525

The vertical elastic design spectral acceleration of X-direction Model 1 is given as follows using:

$S_{ae}(T_p^{(X)}) = \frac{S_{D1}}{T_p^{(Y)}}$ $T_B \leq T_p^{(X)} \leq T_L$

$S_{ae}(0.4846) = \frac{0.095}{0.4846}$ = 0.1960

All calculations for each model across the six floors are carried out in Excel and the resulting values are presented (see Table 8).

Table 8. DD3 Seismic Parameters Per Model

DD3				
Model	$S_{ae}(T_p^{(X)})$ **(g)**	$S_{ae}(T_p^{(Y)})$ **(g)**	S_{DS}	S_{D1}
1	0.196	0.152	0.94	0.255
2	0.159	0.199	0.94	0.255
3	0.201	0.163	0.94	0.255
4	0.209	0.171	0.94	0.255
5	0.199	0.158	0.94	0.255
6	0.194	0.150	0.94	0.255
7	0.207	0.158	0.94	0.255
8	0.180	0.141	0.94	0.255

If the building's fundamental vibration period exceeds the horizontal design spectrum corner period T_B, equation 4 shall be used as the basis for determining the earthquake load reduction coefficient.

$R_a(T_p^{(x)}) = \frac{R}{I}$ $T_B < T_p^{(x)}$

R = 7, I = 1

$R_a(T_p^{(x)}) = \frac{7}{1}$ = 7

$R_a(T_p^{(Y)}) = \frac{R}{I}$ $T_B < T_p^{(Y)}$

R = 7, I = 1 $R_a(T_p^{(Y)}) = \frac{7}{1}$ = 7

All Models are calculated and presented in the table below (see Table 9).

Table 9. **Earthquake Load Reduction Coefficient**

Model	$S_{ae}(T_p^{(X)})$ **(g)**	$S_{ae}(T_p^{(Y)})$ **(g)**	**R**	**I**	T_B	**D**	$R_a(T_p^{(x)})$	$R_a(T_p^{(Y)})$
1	0.526	0.409	7	1	0.27	2.5	7	7
2	0.427	0.534	7	1	0.27	2.5	7	7
3	0.539	0.436	7	1	0.27	2.5	7	7
4	0.560	0.458	7	1	0.27	2.5	7	7
5	0.535	0.424	7	1	0.27	2.5	7	7
6	0.520	0.403	7	1	0.27	2.5	7	7
7	0.555	0.423	7	1	0.27	2.5	7	7
8	0.483	0.377	7	1	0.27	2.5	7	7

The reduced design spectral acceleration is calculated using equation 3 as expressed below:

$S_{aR}(T_p^{(x)}) = \frac{S_{ae}(T_p^{(x)})}{R_a(T_p^{(x)})} = \frac{0.5262}{7} = 0.0751$ $S_{aR}(T_p^{(Y)}) = \frac{S_{ae}(T_p^{(Y)})}{R_a(T_p^{(Y)})} = \frac{0.4095g}{7} = 0.0585g$

The calculated reduced horizontal elastic design spectra for all Models are presented in table 10.

Table 10. Reduced Horizontal Elastic Design Spectra

Model	$S_{ae}(T_p^{(X)})$ (g)	$S_{ae}(T_p^{(Y)})$ (g)	$S_{aR}T_p^{(x)}$	$S_{aR}T_p^{(y)}$
1	0.5262	0.4095	0.0751	0.0584
2	0.42778	0.5349	0.0611	0.0764
3	0.53922	0.4367	0.0770	0.0623
4	0.5604	0.4584	0.0800	0.0654
5	0.53594	0.4242	0.0765	0.0605
6	0.52032	0.4031	0.0743	0.0575
7	0.55563	0.4239	0.0793	0.0605
8	0.48371	0.3775	0.0691	0.0539

3.2 Solution Under Equivalent Seismic Loads

For the total equivalent seismic load (base shear force) according to Equation 12.

$V_{tE}^{(x)}= m_t\, S_{aR}(T_p^{(x)}) \geq 0.4\, m_t$ I S_{DS} g

$V_{tE}^{(Y)}= m_t\, S_{aR}(T_p^{(Y)}) \geq 0.4\, m_t$ I S_{DS} g

m_t is calculated using equation 13

$m_t= \sum_{i=1}^{N} m_i$ mt =3813.192

$V_{tE}^{(x)}$=0.4x3813.192 x 0.0751 x 9.81 ≥ 0.04 x 3813.192 x1 x 0.94 x 9.81

$V_{tE}^{(x)} = 1123.72\ kN \leq 1{,}406.55\ kN$

$V_{tE}^{(x)} = 1{,}406.55\ kN$

$V_{tE}^{(Y)}= m_t\, S_{aR}(T_p^{(Y)}) \geq 0.4\, m_t$ I S_{DS} g

$V_{tE}^{(Y)}$= 3813.192 x 0.0585 x 9.81 ≥ 0.04 x 3813.192 x_1 x 0.94 x 9.81

$V_{tE}^{(Y)} = 2188.076\ kN \geq 1{,}406.55\ kN$

$V_{tE}^{(Y)} = 2188.076\ kN$

The equivalent seismic loads for all Models, calculated in Excel (see Table 11).

Table 11. Equivalent Seismic Loads Per Model

$V_{tE}^{(x)}$ (kN)	$V_{tE}^{(Y)}$ (kN)	limit $V_{tE}^{(x)}$ (kN)	limit $V_{tE}^{(Y)}$ (kN)
2811.99	2188.076	1406.519	1406.519
2285.997	2858.381	1406.519	1406.519
2881.567	2333.628	1406.519	1406.519
2994.739	2449.465	1406.519	1406.519
2864.022	2266.639	1406.519	1406.519
2780.536	2154.288	1406.519	1406.519
2969.231	2265.098	1406.519	1406.519
2584.903	2017.513	1406.519	1406.519

Determination of Equivalent Earthquake Loads Acting on the Floors. The calculated total equivalent earthquake load is expressed as the sum of the equivalent earthquake loads acting on the building floors as shown in equation 16.

$V_{tE}^{x}=\Delta F_{NE}^{X}+\sum_{i=1}^{N} F_{NE}^{(X)}$

The additional equivalent earthquake load acting on the Nth floor (top) of the building, ΔF_{NE}^{X}, will be calculated using equation 17 as follows.

ΔF_{NE}^{X}=0.0075NV_{tE}^{x}

Determination of the equivalent earthquake loads acting on the floors are presented in Table 12.

Table 12. Total Equivalent Seismic Loads for Top Floor

Model	floor number	$V_{tE}^{(x)}$ (kN)	$V_{tE}^{(Y)}$ (kN)	ΔF_{NE}^{X} (kN)	ΔF_{NE}^{y} (kN)
1	6	2811.9901	2188.08	126.5	5.694
2	6	2285.9971	2858.38	102.9	4.629
3	6	2881.5671	2333.63	129.7	5.835
4	6	2994.7385	2449.46	134.8	6.064
5	6	2864.0221	2266.64	128.9	5.710
6	6	2780.5357	2154.29	125.1	5.631
7	6	2969.2309	2265.10	133.6	6.013
8	6	2584.9030	2017.513	116.32	5.234

The remaining part of the total equivalent earthquake load, excluding $\Delta F_{NE}^{(X)}$ will be distributed to the building floors, including the Nth floor, using equation 7.

$F_{IE}^{X}= (V_{tE}^{x}-\Delta F_{NE}^{X})$

Table 13 and Table 14 present the total equivalent earthquake loads for all floors in the X and Y directions, including the top floor, which was calculated previously

Table 13. EX-Direction Total Equivalent Seismic Loads for Model

EX FOR MODEL NO:1						
Floor	h_i **(m)**	H_i **(m)**	w_i **(** kN **)**	m_i $(kN.sec^2/m)$	M_iH_i $(kN.sec^2)$	F_{IE}^X **(** kN **)**
6	3	18	6138	625.67	11262.06	883.5827
5	3	15	6254	637.5	9562.569	642.8025
4	3	12	6254	637.5	7650.055	514.242
3	3	9	6254	637.5	5737.541	385.6815
2	3	6	6254	637.5	3825.028	257.121
1	3	3	6254	637.5	1912.514	128.5605
				3813.2	39949.76	2811.99

Table 14. EY-Direction Total Equivalent Seismic Loads for Model

EY FOR MODEL NO:1						
Floor	h_i **(m)**	H_i **(m)**	w_i **(** kN **)**	m_i $(kN.sec^2/m)$	M_iH_i $(kN.sec^2)$	F_{IE}^X **(** kN **)**
6	3	18	6137.82	625.6697	11262.06	687.5366
5	3	15	6253.92	637.5046	9562.569	500.1799
4	3	12	6253.92	637.5046	7650.055	400.1439
3	3	9	6253.92	637.5046	5737.541	300.1079
2	3	6	6253.92	637.5046	3825.028	200.0719
1	3	3	6253.92	637.5046	1912.514	100.036
				3813.193	39949.76	2188.076

The results for the EX and EY directions in Model 1, both tables show that the seismic loads increase as we move to higher floors, which is expected because the mass and height become larger. The total mass and total seismic load are almost the same in both directions, but the EY direction gives slightly smaller floor forces. This difference comes from small changes in the floor masses and how the building behaves in that direction. The building reacts in a similar way in both EX and EY, and there are no major differences between the two directions.

The maximum and minimum displacements for the EXP load case on Floor 6 of Model 1 were 0.0121 and 0.0073, respectively. Similar EXP, EXN, EYP, and EYN displacements were calculated for each floor, and the results are summarized in table 15 which determines the peak $(d_{\mathrm{i}})_{min}$and $(d_{\mathrm{i}})_{min}$ displacements for each floors of in all four seismic loading directions. (see table 15).

Table 15. Floor Displacements for Model 1

EXP			EXN		
Floor no	$(d_i)_{max}$ (m)	$(d_i)_{min}$ (m)	**floor no**	$(d_i)_{max}$ (m)	$(d_i)_{min}$ (m)
6	0.0121	0.0073	6	0.0121	0.0072
5	0.0096	0.0057	5	0.0096	0.0057
4	0.0071	0.0024	4	0.0071	0.0041
3	0.0046	0.0027	3	0.0046	0.0026
2	0.0024	0.0014	2	0.0024	0.0014
1	0.0008	0.0004	1	0.0008	0.0004
EYP			**EYN**		
Floor no	$(d_i)_{max}(m)$	$(d_i)_{min}$ (m)	**floor no**	$(d_i)_{max}$ (m)	$(d_i)_{min}$ (m)
6	0.0119	0.0095	6	0.0129	0.0092
5	0.0101	0.0081	5	0.0101	0.0078
4	0.0079	0.0063	4	0.0086	0.0062
3	0.0056	0.0044	3	0.0055	0.0043
2	0.0032	0.0026	2	0.0034	0.0025
1	0.0011	0.0009	1	0.0012	0.0009

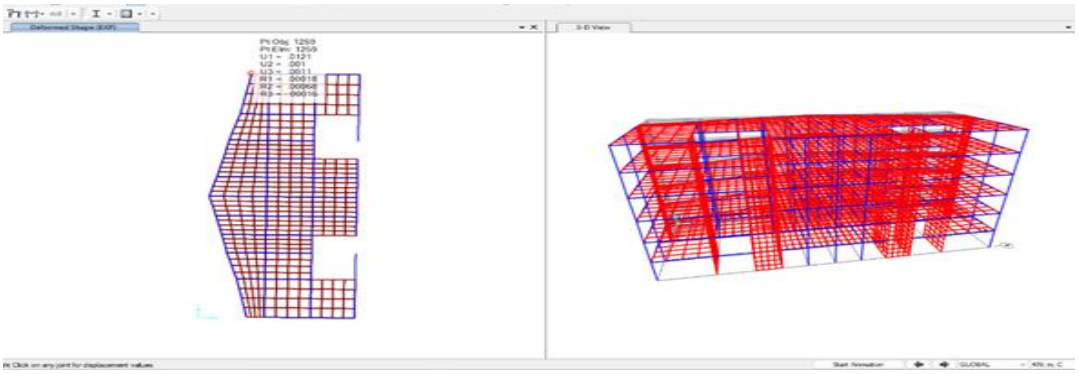

Figure 6. Displacements Under Seismic Load from SAP2000.

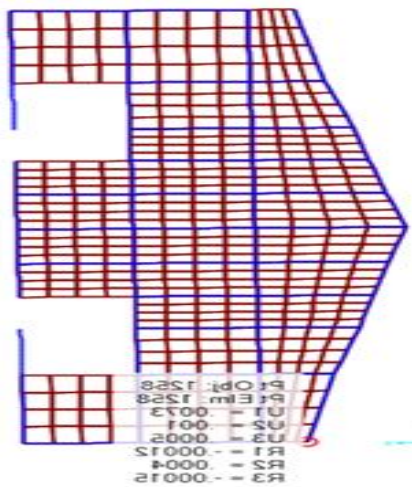

Figure 7. Displacements Under Seismic Loads II from SAP2000.

4. Irregularity Verifications

The results from the linear elastic modal analysis of all eight models were subjected to irregularity checks mandated by TBDY-2018, with detailed results for Model 1 presented below.

4.1 Torsional Irregularity Check for Model 1

For torsional irregularity see Table 16 to Table19.

Table 16. **Model 1 EXP for Torsional Irregularity**

EXP						
Floor no	$(d_i)_{ax}$ (m)	$(d_i)_{min}$ (m)	$(\Delta i)_{max}$ (m)	$(\Delta i)_{min}$ (m)	$(\Delta i)_{avg}$ (m)	η_{bi}
6	0.0121	0.0073	0.0025	0.0016	0.00205	1.2195
5	0.0096	0.0057	0.0025	0.0015	0.002	1.25
4	0.0071	0.0042	0.0025	0.0015	0.002	1.25
3	0.0046	0.0027	0.0022	0.0013	0.00175	1.2571
2	0.0024	0.0014	0.0016	0.001	0.0013	1.2307
1	0.0008	0.0004	0.0008	0.0004	0.0006	1.3333

Table 17. Model 1 EXN for Torsional Irregularity

EXN						
Floor no	$(d_i)_{max}(m)$	$(d_i)_{min}$ (m)	$(\Delta i)_{max}$ (m)	$(\Delta i)_{min}$ (m)	$(\Delta i)_{avg}$ $(m$	η_{bi}
6	0.0121	0.0072	0.0025	0.0015	0.002	1.25
5	0.0096	0.0057	0.0025	0.0016	0.00205	1.2195
4	0.0071	0.0041	0.0025	0.0015	0.002	1.25
3	0.0046	0.0026	0.0022	0.0012	0.0017	1.2948
2	0.0024	0.0014	0.0016	0.001	0.0013	1.2307
1	0.0008	0.0004	0.0008	0.0004	0.0006	1.3333

Table 18. Model 1 EYP for Torsional Irregularity

EYP						
Floor no	$(d_i)_{max}(m)$	$(d_i)_{min}$ (m)	$(\Delta i)_{max}$ (m)	$(\Delta i)_{min}$ (m)	$(\Delta i)_{avg}$ (m)	η_{bi}
6	0.0119	0.0095	0.0018	0.0014	0.0016	1.125
5	0.0101	0.0081	0.0022	0.0018	0.002	1.1
4	0.0079	0.0063	0.0023	0.0019	0.0021	1.09524
3	0.0056	0.0044	0.0024	0.0018	0.0021	1.14286
2	0.0032	0.0026	0.0021	0.0017	0.0019	1.10526
1	0.0011	0.0009	0.0011	0.0009	0.001	1.1

Table 19. Model 1 EYN for Torsional Irregularity

EYN						
Floor no	$(d_i)_{max}$ (m)	$(d_i)_{min}$ (m)	$(\Delta i)_{max}$ (m)	$(\Delta i)_{min}$ (m)	$(\Delta i)_{avg}$ (m)	η_{bi}
6	0.0129	0.0092	0.0028	0.0014	0.0021	1.33333
5	0.0101	0.0078	0.0015	0.0016	0.0015	0.96774
4	0.0086	0.0062	0.0031	0.0019	0.0025	1.24
3	0.0055	0.0043	0.0021	0.0018	0.0019	1.07692
2	0.0034	0.0025	0.0022	0.0016	0.0019	1.15789
1	0.0012	0.0009	0.0012	0.0009	0.0010	1.14286

Model 1 shows torsional irregularity under EXP and EXN loadings, with $\eta_{bi} > 1.2$ on all floors. Maximum floor displacements range from 0.0008 to 0.0121 m, and inter story drifts are between 0.0004 and 0.0025 m. For EYP, η_{bi} stays below 1.2 except at Floor 3, a small irregularity is noticed. Under EYN, torsional irregularity appears at Floors 4 and 6, with displacements up to 0.0129 m. These results indicate clear torsional effects due to the building's structural asymmetry

4.2. Soft Floor Check for Model 1

For soft floor irregularity see Table 20 to Table 23.

Table 20. Model 1 EXP for Soft Floor

EXP					
Floor no	h_i (m)	$(\Delta_i)_{avg}$ (m)	$(\Delta_i)_{avg}/h_i$	η_{ki}	η_{ki}
6	3	0.00205	0.000683	0	1.025
5	3	0.002	0.000667	0.9756098	1
4	3	0.002	0.000667	1	1.14286
3	3	0.00175	0.000583	0.875	1.34615
2	3	0.0013	0.000433	0.7428571	2.16667
1	3	0.0006	0.0002	0.4615385	0

Table 21. Model 1 EXN for Soft Floor

EXN					
Floor no	$h_i(m)$	$(\Delta_i)_{avg}$ (m)	$(\Delta_i)_{avg}/h_i$	η_{ki}	η_{ki}
6	3	0.002	0.000667	0	0.97561
5	3	0.00205	0.000683	1.025	1.025
4	3	0.002	0.000667	0.9756098	1.17647
3	3	0.0017	0.000567	0.85	1.30769
2	3	0.0013	0.000433	0.7647059	2.16667
1	3	0.0006	0.0002	0.4615385	0

Table 22. Model 1 EYP for Soft Floor

EYP					
Floor no	h_i (m)	$(\Delta_i)_{avg}(m)$	$(\Delta_i)_{avg}/h_i$	η_{ki}	η_{ki}
6	3	0.0016	0.000533	0	0.8
5	3	0.002	0.000667	1.25	0.95238
4	3	0.0021	0.0007	1.05	1
3	3	0.0021	0.0007	1	1.10526
2	3	0.0019	0.000633	0.9047619	1.9
1	3	0.001	0.000333	0.5263158	0

Table 23. Model 1 EYN for Soft Floor

EYN					
Floor no	h_i (m)	$(\Delta_i)_{avg}$ (m)	$(\Delta_i)_{avg}/h_i$	η_{ki}	η_{ki}
6	3	0.0021	0.0007	0	1.35484
5	3	0.00155	0.000517	0.7380952	0.62
4	3	0.0025	0.000833	1.6129032	1.28205
3	3	0.00195	0.00065	0.78	1.02632
2	3	0.0019	0.000633	0.974359	1.80952
1	3	0.00105	0.00035	0.5526316	0

The verification of the soft-floor shows that under EXP loading the drift values range from 0.0006-0.00205 m and the drift ratios from 0.0002-0.000683 with a soft floor occurring only at Floor 2 (η_{bi} = 2.166). Under EXN, the drifts are 0.0006-0.00205 and drift ratios 0.0002-0.000683 m, again showing a soft floor at Floor 2 (η_{bi}= 2.166).

For EYP, drift values between 0.001-0.0021 and drift ratios up to 0.0007 give η_{ki} values all below 2, meaning no soft floor. Under EYN, drifts range from 0.00105-0.0025 up to 0.00083, and η_{ki} values also stay below 2. No stiffness irregularity occurs.

4.3 Interstory Drift Control for Model 1.
For this irregularity see Tables 24 to 27.

Table 24. Model 1 EXP for Drift Control

EXP						
Floor no	d_{imax} (m)	$(\Delta_i)_{avg}(m)$	$(d_i)_{max}$ (m)	h_i (m)	λ	**Relative displacement**
6	0.0121	0.0025	0.0175	3	0.372549	0.002173203
5	0.0096	0.0025	0.0175	3	0.142857	0.000833333
4	0.0071	0.0025	0.0175	3	0.142857	0.000833333
3	0.0046	0.0022	0.0154	3	0.142857	0.000733333
2	0.0024	0.0016	0.0112	3	0.142857	0.000533333
1	0.0008	0.0008	0.0056	3	0.142857	0.000266667

Table 25. Model 1 EXN for Drift Control

EYP						
Floor no	d_{imax} (m)	$(\Delta_i)_{avg}(m)$	$(d_i)_{max}$ (m)	$h_i(m)$	λ	**Relative displacement**
6	0.0119	0.0018	0.0126	3	0.372549	0.001564706
5	0.0101	0.0022	0.0154	3	0.142857	0.000733333
4	0.0079	0.0023	0.0161	3	0.142857	0.000766667
3	0.0056	0.0024	0.0168	3	0.142857	0.0008
2	0.0032	0.0021	0.0147	3	0.142857	0.0007
1	0.0011	0.0011	0.0077	3	0.142857	0.000366667

Table 26. Model 1 EYP for Drift Control

EYP						
Floor no	d_{imax} (m)	$(\Delta_i)_{avg}$ (m)	$(d_i)_{max}$ (m)	h_i (m)	λ	**Relative displacement**
6	0.0119	0.0018	0.0126	3	0.372549	0.001564706
5	0.0101	0.0022	0.0154	3	0.142857	0.000733333
4	0.0079	0.0023	0.0161	3	0.142857	0.000766667
3	0.0056	0.0024	0.0168	3	0.142857	0.0008
2	0.0032	0.0021	0.0147	3	0.142857	0.0007
1	0.0011	0.0011	0.0077	3	0.142857	0.000366667

The inter-story drift check shows that the relative drift values remain safely below the limit of 0.008 for all loading directions.

Under EXP and EXN, the relative drifts range from 0.00027 to 0.00217, while EYP produces values between 0.00037 and 0.00156. For EYN, the relative drifts vary from 0.00040 to 0.00243, with the highest value still well under the allowed limit. These results confirm that Model 1 meets the inter story drift requirements of TBDY 2018 in every direction.

4.4 2nd Order Effect for Model 1

Results are presented Table 28 to Table 31.

Table 27. Model 1 EYN Drift Control

Floor no	$d_{imax}\,(m)$	$(\Delta_i)_{avg}$	dimax	hi	λ	Relative displacement
6	0.0129	0.0028	0.0196	3	0.372549	0.002433987
5	0.0101	0.0015	0.0105	3	0.142857	0.0005
4	0.0086	0.0031	0.0217	3	0.142857	0.001033333
3	0.0055	0.0021	0.0147	3	0.142857	0.0007
2	0.0034	0.0022	0.0154	3	0.142857	0.000733333
1	0.0012	0.0012	0.0084	3	0.142857	0.0004

Table 28. Model 1 EXP for 2nd Order Effect

Floor no	$d_{imax}\,(m)$	$m_i\,(t)$	$w_i\,(kN)$	$V_t\,(kN)$	$h_i\,(m)$	$\theta_{II,I}$	Indicator condition
6	0.0121	625.67	6137.8	883.58	3	0.171	0.0857143
5	0.0096	637.5	6253.9	642.80	3	0.186	0.0857143
4	0.0071	637.5	6253.9	514.24	3	0.172	0.0857143
3	0.0046	637.5	6253.9	385.68	3	0.149	0.0857143
2	0.0024	637.5	6253.9	257.12	3	0.116	0.0857143
1	0.0008	637.5	6253.9	128.56	3	0.078	0.0857143

Table 29. Model 1 EXN for 2nd Order Effect

Floor no	$d_{imax}\,(m)$	$m_i\,(t)$	$w_i\,(kN)$	$V_t\,(kN)$	$h_i\,(m)$	$\theta_{II,I}$	Indicator condition
6	0.0121	625.67	6137.8	883.5827	3	0.1708	0.0857143
5	0.0096	637.5	6253.9	642.8025	3	0.1862	0.0857143
4	0.0071	637.5	6253.9	514.242	3	0.1722	0.0857143
3	0.0046	637.5	6253.9	385.6815	3	0.1487	0.0857143
2	0.0024	637.5	6253.9	257.121	3	0.1164	0.0857143
1	0.0008	637.5	6253.9	128.5605	3	0.0776	0.0857143

Table 30. Model 1 EYP for 2nd Order Effect

Floor no	$d_{imax}\,(m)$	$m_i\,(t)$	$w_i\,(kN)$	$V_t\,(kN)$	$h_i\,(m)$	$\theta_{II,I}$	Indicator condition
6	0.0121	625.67	6137.8	883.5827	3	0.1708	0.085714286
5	0.0096	637.5	6253.9	642.8025	3	0.1862	0.085714286
4	0.0071	637.5	6253.9	514.242	3	0.1722	0.085714286
3	0.0046	637.5	6253.9	385.6815	3	0.1487	0.085714286
2	0.0024	637.5	6253.9	257.121	3	0.1164	0.085714286
1	0.0008	637.5	6253.9	128.5605	3	0.0776	0.085714286

Table 31. Model 1 EYN for 2nd Order Effect

Floor no	d_{imax} (m)	m_i (t)	w_i (kN)	V_t (kN)	h_i (m)	$\theta_{II,I}$	Indicator condition
6	0.012	625.6	6137.8	687.5366	3	0.234	0.085714
5	0.010	637.5	6253.9	500.1799	3	0.251	0.085714
4	0.008	637.5	6253.9	400.1439	3	0.268	0.085714
3	0.005	637.5	6253.9	300.1079	3	0.228	0.085714
2	0.003	637.5	6253.9	200.0719	3	0.211	0.085714
1	0.001	637.5	6253.9	100.036	3	0.149	0.085714

For Model 1, 2nd order effect, the values were compared with the TBDY 2018 limit of 0.0857. In the EXP and EXN directions, 2nd order effect ranges between 0.116-0.186, so all floors except the 1st floor (≈ 0.078) require second-order effects.

The EYP results are the same, with only the ground floor meeting the limit. In the EYN direction, θ values are much higher (0.1496-0.268), meaning every floor exceeds the limit and second-order effects must be considered throughout the whole building.

The same process should be followed for each model in order to verify floor by floor according to TBDY 2018.

Conclusion and recommendation

This research demonstrated how the geometric shape of reinforced concrete affects its seismic behavior. By analyzing eight structural models in SAP2000 according to TBDY-2018, we were able to obtain the results showing that geometry has a major impact on structural performance. Regular and symmetrical buildings responded better to earthquakes, with lower torsional effects, smaller displacements, and more controlled inter-story drifts. Models with irregularities such as asymmetric plans or uneven stiffness distribution presented larger lateral movements, increased torsion, and higher stress concentrations, which make them more vulnerable during strong ground motion. The geometry influenced the dynamic properties such as the fundamental period and base shear since irregular buildings generally had longer periods and greater seismic requirements. The Turkish Seismic Code provided consistent guidance for evaluating these behaviors.

To obtain more realistic responses in other research, the use of real earthquake records is recommended. Comparing TBDY-2018 with international codes like Eurocode 8, ASCE 7, IS 1893, and NZS 1170.5 could help identify differences in design approaches. Further studies may also include soil structure interaction, high-rise or complex building forms, and advanced materials such as high-strength concrete or hybrid RC steel systems. Additionally, machine learning methods could be used to explore more efficient geometric configuration and improve earthquake-resistant design methods.

References

[1] Suliman, M., and Lu, L. (2024).A Comparative Study of Seismic Performance Evaluation of Reinforced Concrete Frame Structures Using Chinese and African Seismic Codes. *Advances in Civil Engineering*, 2024(1), 5588833.

[2] Santos, s., giarlelis, c., traykova, m., lima, s., bucur, c., and orrala, w. comparative study of some Seismic codes for building design regarding criteria for non-linear methods of analysis.

[3] Rajeev, A., Meena, N. K., and Pallav, K. (2019). Comparative study of seismic design and performance of OMRF building using Indian, British, and European codes. *Infrastructures*, 4(4), 71.

[4] Kunwar, S., Thapa, D., Paudel, A., and Shrestha, A. (2024). Discover Civil Engineering. Discover, 1, 117.

[5] Bhavsar, M. J., Choksi, K. N., Bhatt, S. K., and Shah, S. K. (2014). Comparative study of typical RCC building using Indian standards and Euro standards under seismic forces. *International Journal of Scientific and Research Publications, 4(12), 1-4.*

[6] Landingin, J., Rodrigues, H., Varum, H., Arêde, A., and Costa, A. (2013). Comparative analysis of RC irregular buildings designed according to different seismic design codes.

[7] Ergün, A., Kıraç, N., and Başaran, V. (2015). The evaluation of structural properties of reinforced concrete building designed according to pre-modern code considering seismic performance. *Engineering Failure Analysis*, 58, 184-191.

[8] Hassan, A., and Pal, S. (2018). Effect of soil condition on seismic response of isolated base buildings. *International Journal of Advanced Structural Engineering*, 10(3), 249-261.

[9] Resatoglu, R., and Hamed, M. (2019). Comparative study of Different Seismic Codes for Reinforced Concrete Buildings in Northern Cyprus Using Static and Dynamic

Methods. *Journal of Engineering Science and Technology*,14(3), 1314-1329.

[10] Tabsh, S. W. (2013). Comparison between reinforced concrete designs based on the ACI 318 and BS 8110 codes. *Structural Engineering and Mechanics*, 48(4), 467-477.

[11] Izhar, T., and Dagar, R. (2018). Comparison of reinforced concrete member design methods of various countries. *International Journal of Civil Engineeringand Technology (IJCIET)*, 9(4), 637-646.

[12] Bashir, S. (2014). Design of Short Columns According to ACI 318-11 and BS 8110-97: A Comparative Study Based on Conditions in Nigeria (Doctoral dissertation, Near East University).

[13] Kurç, Ö., Kayışoğlu, B., Lüleç, A., and Özcebe, G. (2011). A comparative study on structural wall design approach of 2007 Turkish earthquake code. *Teknik Dergi*, 22(110), 1477-1497.

[14] Gullu, M. F., and Mohammed, F. S. (2021). Investigating the reliability of shear strength equations in TS500 and ACI318-19. *Journal of Structural Engineering*, 4(2), 057-067.

[15] Amulu, C. P., and Ezeagu, C. A. (2017). Experimental and analytical comparison of torsion, bending moment and shear forces in reinforced concrete beams using BS 8110, euro code 2 and ACI 318 provisions. *Nigerian Journal of Technology, 36(3), 705-711*.

[16] Uzel, A. (2019). Evaluation of TS500-2000 Shear Strength Provisions for Deep Beams. Süleyman Demirel Üniversitesi Fen Bilimleri Enstitüsü Dergisi, 23(2), 338-342.

[17] Gowrishankar, P. (2018). Critical Review of Reinforced Concrete Design Codes and Their Relevance to the United Arab Emirates (Master's thesis, The British University in Dubai).

[18] Nwoji, C. U., and Ugwu, A. I. (2017). Comparative Study of BS 8110 and Eurocode 2 in structural design and analysis. *Nigerian Journal of Technology*, 36(3), 758-766.

[19] Zhang, L., Hu, H., Fang, Y., and Qiang, Z. (2021). Code compliance in reinforce concrete design: A comparative study of USA code (ACI) and Chinese code (GB). *Advances in Civil Engineering*, 2021(1) 5517332.

[20] Algott, I. H., and Kafri, G. M. A. (2023). Comparative Study of Reinforced Concrete Design of Short Columns between BS 8110 and ACI 318-11 (Codes). *Sirte University Scientific Journal*, 13(1), 46-54.

[21] Adhav, A., Gawande, G., Vishwakarma, S., Dhapekar, K., and Moon, N. (2019). Comparative study of analysis and design of building using indian standards (IS), European norms (EN) and American concrete institute (ACI). *Int J Res Appl Sci Eng Technol*, 7, 1436-1442.

[22] Nwofor, T., Sule, S., and Eme, D. B. (2015). A comparative study of Bs8110 and Eurocode 2 standards for design of a continuous reinforced concrete beam. *International journal of civil engineering and technology*, 6(5), 76-84.

[23] Oussadou, S. E. (2021). Comparison of the Provisions of ACI318-19 Code and Eurocode on the Structural Design and Cost Analysis, of a High-Rise Concrete Building Subjected to Seismic and Wind Forces (Master's thesis, The British University in Dubai).

[24] Jayasinghe, T., Gunawardena, T., and Mendis, P. (2021). A comparative study on minimum shear reinforcement provisions in codes of practice for reinforced concrete beams. *Case Studies in Construction Materials*, 15, e00617.

[25] Ahmad, M. M., Elahi, A., and Barbhuiya, S. (2023). Comparative Analysis of Reinforced Concrete Beam Behaviour: Conventional Model vs. Artificial Neural Network Predictions. Materials, 16(24), 7642.

[26] Araújo, D. L., Silva Neto, A. P., Lobo, F. A., and El Debs, M. K. (2016). Comparative analysis of design models for concrete corbels. Revista IBRACON de Estruturas e Materiais, 9, 435-470.

[27] Caterino, N., Di Cristo, V., and Ceroni, F. (2024). Strength capacity of RC beams without shear reinforcement: Numerical analysis and comparisons with code provisions. Engineering Structures, 317, 118634.

[28] Hamrat, M., Boulekbache, B., Tahenni, T., Chemrouk, M., and Amziane, S. (2022). Experimental study of deflection of steel fibre reinforced concrete beams: comparison of different design codes. *European Journal of Environmental and Civil Engineering*, 26(6), 2057-2073

[29] Lee, Y. H., Kim, M. S., Lee, J., and Scanlon, A. (2013). Comparison of minimum thickness provisions for concrete beams in building codes and standards. Canadian Journal of Civil Engineering, 40(7), 595-602.

[30] Kiani, A., Yang, T. Y., KheyroDdin, A., Kafi, M. A., and Naderpour, H. (2024, March). Quantification of seismic performance factors of mixed concrete/steel buildings using the FEMA P695 methodology. *In Structures* (Vol.61, p. 06144). Elsevier.

[31] Yang, K. H., and Ashour, A. F. (2008). Code modelling of reinforced-concrete deep beams. *Magazine of Concrete Research, 60(6), 441-454.*

[32] Bernard, E. S., Amin, A., and Gilbert, R. I. (2020). Assessment of MC2010 and AS3600 models for

estimating instantaneous flexural crack widths in fibre reinforced concrete members. *Engineering Structures*, 208, 110271.

[33] Pacheco, J., De Brito, J., Chastre, C., and Evangelista, L. (2019). Uncertainty models of reinforced concrete beams in bending: Code comparison and recycled aggregate incorporation. *Journal of StructuralEngineering*, 145(4), 04019013.

[34] Kabashi, N., Avdyli, B., Krasniqi, E., and Këpuska, A. (2020). Comparative approach to flexural behavior of reinforced beams with GFRP, CFRP, and steel bars. *Civil Engineering Journal*, 6(1), 50-59.

[35] Li, H., Pan, Z., Yang, Y., Wang, X., Tang, H., Ma, F., and Zheng, L. (2024). Predicting Residual Flexural Strength of Corroded Prestressed Concrete Beams: Comparison of Chinese Code, Eurocode and ACI Standard. *Buildings*, 14(7), 2047.

[36] Izhar, T., Bano, S., & Mumtaz, N. (2019). Comparative study on analysis and design of reinforced concrete building under seismic forces for different codal guidelines. *Int J Trend Sci Res Dev*, 3(4), 536-551.

[37] Sezen, H., Whittaker, A. S., Elwood, K. J., and Mosalam, K. M. (2003). Performance of reinforced concrete buildings during the August 17, 1999 Kocaeli, Turkey earthquake, and seismic design and construction practise in Turkey. *Engineering Structures*, 25(1), 103-114.

[38] Fragomeni, S., & Loo, Y. C. (2003). Asian concrete model code (ACMC) and Australian concrete structures standard (AS3600) compared. Australian Journal of Structural Engineering, 4(3), 177-185

[39] Workeluel, N., Saha, P., Matiyas, S., and Mohanty, T. (2023). A comparative study on analysis and design of RC C elevated water tank using different country codes. Materials Today: Proceedings.